A comparison of self-potential tomography with electrical resistivity tomography for the detection of abandoned mineshafts.

Paul B. Wilkinson[1], Jonathan E. Chambers[1], Philip I. Meldrum[1], Richard D. Ogilvy[1], Chris J. Mellor[2] and Simon Caunt[3].

[1] British Geological Survey, Kingsley Dunham Centre, Keyworth, Nottingham, NG12 5GG, UK

[2] School of Physics and Astronomy, University of Nottingham, Nottingham, NG7 2RD, UK

[3] The Coal Authority, 200 Lichfield Lane, Mansfield, NG18 4RG, UK

Abstract

We present a comparison of the abilities of Electrical Resistivity Tomography (ERT) and Self-Potential Tomography (SPT) to detect and characterize buried mineshafts at the site of a former colliery. Surface electrical resistivity and self-potential (SP) surveys were carried out at two test sites, each containing a hidden shaft. The ERT survey results indicate that both sites had a highly heterogeneous subsurface resistivity distribution, which we attribute to colliery spoil and former infrastructure. ERT managed to distinguish an air-filled, highly resistive mineshaft from this background, but failed to detect the second shaft, which was backfilled and therefore had a much lower resistivity contrast with the surrounding formation. However, SPT located both shafts, gave an indication of their size, shape and depth of burial, and was able to distinguish the open- from the backfilled mineshaft due to the strength of the associated SP anomalies. We argue that these SP anomalies are likely to be due to changes in the streaming potential caused by preferential drainage into the shafts.

Introduction

The measurement of the spontaneously occurring electrical self-potential (SP) has been used for many years as a geophysical survey technique, chiefly in the area of mineral prospecting. Recently there has been renewed interest in the use of SP data for geohazard monitoring (Patella, 1997b; Perrone *et al*., 2004). But, despite the fact that SP surveying is quick and inexpensive, its use in environmental and engineering site investigation has not been widely appreciated (Nyquist and Corry, 2002). This is most likely due to an incomplete understanding of the causative mechanisms of SP anomalies in the context of contaminated land or engineering sites. These can include diffusion-, electrofiltration-, mineral-, thermal-, bioelectric- and streaming potentials. Although recent advances have been made by studying these effects in isolation (Titov *et al*., 2002; Reppert and Morgan, 2003; Naudet *et al*., 2003; Guichet *et al*., 2003), the decoupling of the various SP mechanisms is not trivial (Revil *et al*., 2003). Due to the wide use of SP surveying in mineral exploration, many existing analysis techniques tend to fit data to forward models representing isolated mineral deposits. These are based on charged geometric structures such as planes, rods and ellipsoids (Cooper, 1997; Abdelrahman *et al*., 2003). Fortunately, a few self-potential tomography techniques are now emerging which require no *a priori* assumptions about the causative mechanisms or subsurface geometry (Fournier, 1989; Patella, 1997a; 1997b; Gibert and Pessel, 2001; Sailhac and Marquis, 2001).

In this paper, we present a comparison of the efficacy of electrical resistivity tomography (ERT) and self-potential tomography (SPT) in locating and imaging hidden mineshafts. This work was carried out as part of a wider investigation for the Coal Authority into geophysical techniques for the detection of abandoned mine entries. Two test sites were provided, containing buried mineshafts at undisclosed locations. Surface electrical resistivity and SP surveys were conducted at both sites. ERT and SPT techniques were used to produce tomograms of the subsurface, which gave information on the location, size and fill material of the mineshafts.

Site description

Two test sites, known as Site B and Site C, were selected for the trial (see Fig. 1). Site B represented a "greenfield" site, and Site C a "brownfield" site. They were both located in an agricultural area on the site of the former Pewfall Colliery in the north-west of England. Each site contained one mineshaft, of diameter <5 m, in an undisclosed location. One of the shafts had been backfilled whilst the other was open, but the identity of each was unknown at the time of the surveys. The sites had both been leveled and the mine openings re-capped with wooden cappings and buried again. A concrete collar had been used to support the cap of the open shaft. The water table was approximately 32 m below ground level, so it was expected that the open shaft would be air-filled. The topography of both sites was measured, with the elevation data recorded on a regular surface grid with 4 m spacing.

A 50 × 50 m grid was deployed over Site B on a gentle, south-west facing slope. The x-axis of the grid was oriented along E 23° S, and the elevation range across the grid was 2.4 m. The site is cut by the north-west trending Bullstake Fault (Jones *et al*., 1938). To the south of the fault, the bedrock material consists of Middle Coal Measures Formation sedimentary units; to the north, the site is underlain by Ravenhead Rock sandstone. The bedrock has a general dip of 5° to the south-east and it is overlain by a glacial till of unknown thickness. However, the till was recorded to be 3.6 m thick in a borehole situated a short distance from the site. The expected resistivities of the bedrock and till were of the order of 10-100 Ωm, whereas the resistivities of any made ground and backfill material were unknown at the time of the survey. The north-eastern half of the site is covered by the remnants of a former spoil heap, which was found to be up to 3 m thick during site excavations, and the south-western corner of the site was encroached upon by a temporary gravel track. A photograph of Site B is shown in Fig. 2a.

Site C was also surveyed over a 50 × 50 m grid with its x-axis aligned along E 3° S. The site has a gentle, south-east facing slope and an elevation range of 3.1 m. On this site, the bedrock geology consists principally of Lower Coal Measures Formation shales, dipping 5° to the south-east. The north-west corner of the site is underlain by Ravenhead Rock sandstone. It was anticipated that the till cover was approximately 3 to 4 m, thick based on the record of the nearby borehole. The south-western corner of the site is also encroached upon by the remains of the same spoil heap as at Site B. Fig. 2b shows a photograph of Site C.

ERT data acquisition and results

ERT is an established technique for environmental and engineering site investigation (Ogilvy *et al.*, 1999; Chambers *et al.*, 2002; Dahlin *et al.*, 2002; Zhou *et al.*, 2002). Specifically, it has been used to survey for uncharted mine galleries (Maillol *et al.*, 1999) and subsurface cavities (van Schoor, 2002). For our surveys, an automated 8-channel AGI SuperSting R8 IP system was used to collect resistivity data at each site on a 50×50 m grid with electrode spacings of 1 m. A dipole-dipole configuration, with '*a*-spacings' of 1, 2, and 3 m and '*n*-levels' of 1 to 8 (Parasnis, 1997), was used for each survey line on both sites. This configuration was selected for its high lateral resolution and compactness, since the use of arrays with remote electrodes is not practical for small sites. The Site B survey comprised 51 lines parallel to the *x*-axis at 1 m intervals, and an additional 6 orthogonal tie-lines parallel to the *y*-axis at $x = 2, 4, 6, 44, 46$ and 48 m. Site C was surveyed in a similar manner, with 51 lines parallel to the *y*-axis at 1 m intervals and 6 orthogonal tie-lines at $y = 2, 4, 6, 44, 46$ and 48 m. In each case, the tie-lines were introduced to improve the data density at the ends of the main set of 51 data lines.

The electrical resistivity data from the individual lines were joined into a single data set for each site, each with ~34,000 measurements. A small fraction (0.16%) of the measurements with negative or outlying apparent resistivity values were dropped from the site B data set. These measurements were probably affected by poor electrical contact in the area of the graveled road. Similarly, 0.26% of the Site C measurements were also removed. The data sets were inverted using the Res3DInv software package (Loke and

Barker, 1995), using an L_1-norm (robust) regularized optimization method (Ellis and Oldenburg, 1994; Loke and Lane, 2002). The forward problem was solved using a finite-element method to allow for the inclusion of the site topography. Acceptable convergence between the observed and model resistivity data was achieved for both sites as indicated by RMS errors of 2.2% for Site B and 2.8% for Site C.

The 3D ERT model for Site B is shown in Fig. 3a as a series of horizontal sections at different heights, z, extending to 5.0 m below the surface. The origin of the vertical scale is taken to be the lowest point on the Site B survey grid. The upper 2.5 m of ground are highly heterogeneous, which is consistent with the presence of disturbed material or made ground as confirmed by the earlier excavations. Below this, the resistivities tend to be higher towards the west (smaller x). Within the upper section, the trend is reversed, with higher resistivities to the east. The boundary between the low and high resistivity areas cuts roughly diagonally across the grid from the north-western to the south-eastern corner. This boundary coincides with the edge of the spoil heap from historical records (Fig. 1).

A strong, localized conductive anomaly appears between $z = 0$ m and $z = -1$ m as a small yellow/red region centered on ($x = 30$ m, $y = 31$ m). The shallow position, limited vertical extent and highly conductive nature of this feature suggest that it is man-made and is probably due to a buried metal object. There are a large number of resistive anomalies in the model, but few extend deeper than 2 m below ground level. Of these, the anomaly highlighted by the dashed white cylinder centered on ($x = 28$ m, $y = 14$ m) is

most likely to represent the mineshaft. Unlike other vertically persistent anomalies, its lateral dimensions are consistent with the known diameter of the shaft (<5 m) and it does not appear to be connected to any regional trends within the survey area (see magnified section inset in Fig. 3a). Since the anomaly is highly resistive, with a contrast of ~50:1 with respect to the background, this strongly indicates that the shaft was either open and air-filled, or contained highly resistive backfill material.

The Site C model (Fig. 3b) also shows a highly heterogeneous subsurface to roughly 3 m below ground level, consistent with the presence of colliery spoil. Below this there is a general trend of decreasing resistivity with depth. The likely cause of this trend is a change from resistive surficial fill materials to more conductive bedrock. Below $z = 0$ m (the lowest point on the Site C grid), several localized conductive anomalies are present, possibly indicating man-made or waste materials such as buried metal objects, ash or concentrations of aqueous contaminants. Between $z = -1$ m and $z = -3$ m there is a set of marked north-south linear features which extend across the model. These features coincide with the historical locations of colliery buildings and rail tracks (shown on the $z = -2$ m slice by solid white lines). However, there are no anomalies that can be readily associated with a mineshaft. This can clearly be seen in the inset in Fig. 3b, which shows a magnification of the region surrounding the shaft. This indicates that there was little resistivity contrast between the Site C mineshaft and the surrounding bedrock. Consequently the inverted resistivity distribution is dominated by the highly heterogeneous nature of the subsurface. The lack of a high contrast anomaly makes it

very likely that the Site C shaft was backfilled, and hence the shaft at Site B must have been open (rather than being filled with resistive material).

SP theory

In contrast to ERT, where an applied potential difference is used to drive a current through the ground, SP surveying measures potential differences that occur spontaneously. These potentials can be due to a variety of sources, which are often unknown. However, an SPT algorithm has recently been introduced (Patella, 1997a; 1997b; 1998) that makes no *a priori* assumptions about the causative mechanisms of the SP distribution. It calculates the correlation between the observed surface potentials and the potential from a scanning test charge. This technique has successfully been used to map the subsurface charge distributions of the Vesuvius volcano (Patella, 1997b) and the Varco d'Izzo landslide (Perrone *et al*., 2004).

Cross-correlation SPT considers the surface potential to be due to a collection of charge distributed at discrete points beneath the surface. A Poisson equation,

$$\nabla^2 V = -\rho \nabla \cdot \mathbf{J} - \frac{\mathbf{E} \cdot \nabla \rho}{\rho}, \qquad (1)$$

relates the self-potential *V,* and its associated electric field **E**, to the primary sources of current $\nabla \cdot \mathbf{J}$ and the charge build-up at discontinuities in the resistivity distribution ρ. For

a flat surface, the solution to (1) is given by the standard solution of Poisson's equation in a half-space:

$$V = \frac{1}{2\pi} \int_v \frac{1}{r} \left(\rho \nabla \cdot \mathbf{J} + \frac{\mathbf{E} \cdot \nabla \rho}{\rho} \right) dv , \qquad (2)$$

where v is the subsurface volume and r is the distance between the observation point on the surface and the source point in the subsurface. The left-hand term in the bracket is non-zero only at primary sources or sinks of current. The right-hand term is due to secondary charge that accumulates when current flows through resistivity inhomogeneities. If the resistivity is assumed to be constant except for abrupt changes across arbitrarily located interfaces in the subsurface then the second term is non-zero only on these interfaces. The integrals over each interface can then be approximated as sums over small surface elements, each with constant r. Therefore, to a good approximation, V can be considered to be a sum of terms, all of which are proportional to $1/r$, due to charges located at various discrete points in the subsurface (Patella, 1997a). The Charge Occurrence Probability (COP) η at a given subsurface point is found by calculating a cross-correlation integral between the observed electric field ($\mathbf{E} = -\nabla V$) and the field of a unit test charge at that point in a homogeneous medium. The COP lies in the range $-1 \leq \eta \leq 1$, where a large magnitude indicates an increased likelihood that charge

has accumulated at that point, and a negative value simply implies that the accumulated charge is negative.

The self-potential tomograms in this paper were produced by calculating $\eta(x, y)$ for a number of discrete depths. The algorithm is based on a modification of the above technique that allows for the inclusion of topography (Patella, 1997b; 1998). Compared to the published method, higher order numerical approximations (Wilkinson *et al*., 2001) to the cross-correlation integrals and derivatives of V were used. This improved the contrast between low and high values of η in the tomograms by 10%-20% compared to those produced by the standard algorithm. Since a homogeneous medium is assumed for the calculation of the cross-correlation integral, both primary and secondary sources will be present in the SP tomogram. It should be possible to correct for a known resistivity distribution and thereby remove the secondary sources (Sailhac *et al*., 2003). But due to the limited depth of investigation of the ERT surveys compared to the SPT surveys, and also because of the highly heterogeneous nature of both sites, these calculations are beyond the scope of the current paper.

It is known that SP anomalies above cavities can arise due to water flow into the void space, which affects the streaming potential given by the Helmholtz-Smoluchowski equation (Nyquist and Corry, 2002; Vichabian and Morgan, 2002). The SP survey presented here was conducted in early 2004, during and following periods of extensive rainfall. The ground was saturated and the overall drainage at both sites was noticeably poor. Under similar conditions, when the sites were prepared and the shafts were capped,

it was noted that "water was pouring down the walls of the open mineshaft" (Gaskell, 2004). Due to this strong preferential drainage into the shaft, we expected that there would be an associated streaming potential anomaly. Whilst several other studies have presented SP data showing anomalies above subsurface cavities (Lange and Barner, 1995; Quarto and Schiavone, 1996; Zhou *et al*., 1999; Lange, 1999), to the best of our knowledge 3-D self-potential tomography has not previously been applied to this type of investigation. The advantage of using SPT is that it becomes possible to extract information about the shape and depth of burial of the cavity, in addition to finding its location.

SPT data acquisition and results

Measurements of the self-potential were taken using a roving electrode at 2 m intervals with $0 \text{ m} \leq x \leq 50 \text{ m}$, $0 \text{ m} \leq y \leq 48 \text{ m}$ for Site B and $0 \text{ m} \leq x \leq 50 \text{ m}$, $0 \text{ m} \leq y \leq 50$ m for Site C, a total of ~650 measurements at each site. A standard non-polarizing $Cu/CuSO_4$ porous pot reference electrode was located at a fixed point ~5 m outside the grid. The non-polarizing roving electrode had a conical Tufnol nose containing $CuSO_4$, with holes filled with a porous material to make contact with the ground, similar to that shown in Telford (1990). A high-impedance digital voltmeter was used to measure the potential difference between the electrodes. Regular readings were taken in a water bath to correct for potential drift between the electrodes and several of the survey measurements were repeated at regular intervals to compensate for any time-

varying background potential. The electrode drift was found to be ~2 mV during the site B survey and ~6 mV for site C. The variation of the background potential was found to be negligible.

Figure 4 shows plots of the measured SP data, after drift correction, for sites B and C. The black region near the origin in Fig. 4a (Site B) is due to the gravel track that prevented good electrical contact between the ground and the roving electrode. One point at the edge of the road where contact was made (x = 12 m, y = 8 m) was also removed from the data set since it gave non-repeatable readings. There are three reasonably well isolated negative SP anomalies over Site B: a strong, roughly circular feature at (x = 27 m, y = 29 m), a slightly weaker, roughly circular feature at (x = 29 m, y = 14 m) and another weaker, more irregular feature at (x = 14 m, y = 44 m). Over Site C (Fig. 4b), there are many more anomalies that are less well isolated and more irregular. The strongest of these are negative potentials at (x = 30 m, y = 36 m) and (x = 49 m, y = 48 m) and neighboring regions of negative and positive potential at (x = 47 m, y = 21 m) and (x = 45 m, y = 5 m).

A more detailed analysis of the data is presented in Fig. 5. Self-potential tomograms were calculated by evaluating the COP as a function of position and depth for both sites. The topography of the sites was included in the analysis, and the vertical coordinate, z, was taken to be zero at the lowest point on each grid. For Site B (Fig. 5a) there are three distinct features corresponding to the three features in the SP contour plot (Fig. 4a). The elongated feature at (x = 14 m, y = 44 m) is relatively weak and decays

quite quickly with depth. The strong concentration of COP at (x = 27 m, y = 29 m) is more interesting. It has a strong signature at the surface (z = +1m) and decays very rapidly, becoming almost indistinguishable by z = -4 m. This feature corresponds directly with the nearby conductive anomaly identified in the ERT survey and may be due to electrochemical reactions of metallic debris. The final region of enhanced COP at (x = 29 m, y = 14 m) has a different depth dependence, being strongest around z = -2 m to z = -3 m, and persisting to at least z = -10 m. The geometry of this feature is highlighted by a 3 m diameter cylinder, shown by white dashed lines in Fig. 5a. Of the three features, this is the most likely to be associated with the mineshaft, which is known to have been buried to at least 1 m below ground level. Based on the previous observation of strong preferential drainage into the open mineshaft, and the similar saturated ground conditions at the time of the SP survey, it is likely that this feature is due to an anomaly in the streaming potential caused by water flowing into the shaft. The exact mechanisms controlling this flow are not well understood, though they are likely to be dominated by vertical infiltration of surface water into the shaft. The negative sign of the anomaly is consistent with other reports of negative SP anomalies due to downward infiltration into caves and sinkholes (Lange and Barner, 1995; Quarto and Schiavone, 1996; Zhou *et al*., 1999; Lange, 1999).

The SP plot for Site C (Fig. 4b) is much more irregular and cluttered, but the COP analysis (Fig. 5b) has also managed to identify the mineshaft at this site. There are two strong negative concentrations of COP at (x = 45 m, y = 22 m) and (x = 42 m, y = 7 m).

Although the larger of these features persists with depth, they are both strong at the surface and irregularly shaped, unlike the anomaly associated with the shaft at Site B. The causative mechanism for these anomalies is unclear. There is also a positive COP feature at ($x = 48$ m, $y = 3$ m). This appears to be a shallow feature similar to the shallow negative feature at ($x = 27$ m, $y = 29$ m) on Site B. The final strong anomaly is located at ($x = 30$ m, $y = 36$ m) and has a remarkably similar shape and depth dependence to the concentration of COP caused by the mineshaft at Site B. It is close to circular, has a maximum between $z = -2$ m and $z = -3$ m, and it persists to $z = -10$ m. The main difference is that the amplitude of this feature is only half that of the Site B shaft anomaly. Since the magnitude of the streaming potential anomaly is directly proportional to infiltration rate (Erchul and Slifer, 1987), it is very probable that the water flow into this shaft was less than into the shaft at Site B. In turn, it is to be expected that a backfilled mineshaft would provide a weaker preferential drainage route than an open shaft. Using this interpretation, it is highly likely that the backfilled shaft was the cause of the Site C anomaly, whilst the stronger anomaly at Site B was due to the open shaft. This is in agreement with the analysis of the ERT data.

Thus, the use of SPT has successfully located both shafts and has been able to distinguish them from surrounding SP anomalies based on their shape and depth dependence. It was also able to distinguish the fill types of the shafts by comparing the amplitudes of their associated tomographic features. By contrast, ERT located just one of the shafts and was able to distinguish it to only one-third the depth obtained from the SPT

survey. Although ERT was less successful in identifying the positions of the shafts, it did provide additional information not present in the SPT images regarding the extent and thickness of the spoil and the position of former colliery infrastructure. Hence, SPT and ERT imaging were found to be complementary for the wider site investigation problem.

As a final check on the accuracy of the shaft locations, Fig. 6 shows an aerial photo of the site taken before the shaft heads were leveled and buried. The tree-filled regions around the tops of the shafts are circled with white dashed lines. The locations of the streaming potential anomalies associated with the shafts are marked with circles and the centers of the shafts obtained from Ordnance Survey maps are shown as triangles. It can be seen that the positions located by SPT are in agreement to within 2 m. The positions and fill characteristics of the shafts were subsequently confirmed by the Coal Authority.

Conclusions

Surface electrical resistivity and self-potential surveys were conducted at two test sites each containing an abandoned mineshaft. Although ERT successfully identified many features of the shallow subsurface of both sites, it only managed to distinguish the air-filled shaft. The failure to distinguish the second, backfilled, shaft was due the low resistivity contrast between this shaft and the surrounding material and also to extensive subsurface heterogeneity at the second site. By comparison, SPT located *both* shafts accurately and gave a realistic depiction of their shape and depth dependence. It also

enabled the open and backfilled mineshafts to be distinguished by the relative amplitudes of their associated tomographic features, which we attribute to changes in the streaming potential caused by preferential drainage into the shafts. Whilst previous studies have observed streaming potential anomalies due to subsurface cavities, by using SPT we have shown that quantitative information about the cavity can also be obtained.

SPT is a very rapid and inexpensive geophysical survey technique. In this study only ~650 SP measurements were required to create an image of the mineshaft on each site, compared to some 34,000 electrical resistivity measurements. SP surveys are often regarded as auxiliary to other geoelectrical techniques, but this study has demonstrated that they can provide useful diagnostic data, even in situations that present a challenge to other methods. The striking success of SPT in locating both mineshafts suggests that this method deserves wider recognition and application.

Acknowledgements

References

Abdelrahman, E.M., El-Araby, T.M., Hassaneen, A.-R.G., and Hafez, M.A., 2003, New methods for shape and depth determination from SP data: Geophysics, **68**, 1202-1210.

Chambers, J.E., Ogilvy, R.D., Kuras, O., Cripps, J.C., and Meldrum, P.I., 2002, 3D electrical imaging of known targets at a controlled environmental test site: Environmental Geology, **41**, 690-704.

Cooper, G.R.J., 1997, SPINV: Self-potential data modelling and inversion: Computers and Geosciences, **23**, 1121-1123.

Dahlin, T., Bernstone, C., and Loke, M.H., 2002, A 3-D resistivity investigation of a contaminated site at Lernacken, Sweden: Geophysics, **67**, 1692-1700.

Ellis, R.G., and Oldenburg, D.W., 1994, Applied Geophysical Inversion: Geophysical Journal International, **116**, 5-11.

Erchul, R.A. and Slifer, D.W., 1987, The use of spontaneous potential in the detection of groundwater flow patterns and flow rate in karst areas: In Beck BF (Ed.) Proceedings of the 2nd multidisciplinary conference on sinkholes and the environmental impacts of karst, Orlando, Florida.

Fournier, C., 1989, Spontaneous potentials and resistivity surveys applied to hydrogeology in a volcanic area: Case history of the Chaîne des Puys (Puy-de-Dôme, France).: Geophysical Prospecting, **37**, 647-668.

Gaskell, P., Wardell Armstrong Ltd., Newcastle-under-Lyme, UK, Private Communication, 2004.

Gibert, D., and Pessel, M., 2001, Identification of sources of potential fields with the continuous wavelet transform: Application to self-potential profiles: Geophysical Research Letters, **28**, 1863-1866.

Guichet, X., Jouniaux, L., and Pozzi, J.-P., 2003, Streaming potential of a sand column in partial saturation conditions: Journal of Geophysical Research, **108(B3)**, 2141.

Jones, R.C.B., Tonks, L.H., and Wright, W.B., 1938, Wigan District: Memoir of the Geological Survey of Great Britain, One-inch Geological Sheet **84** New Series (England and Wales).

Lange, A.L., 1999, Geophysical studies at Kartchner Caverns state park, Arizona: Journal of Cave and Karst Studies, **61**, 68-72.

Lange, A.L., and Barner, W.L., 1995, Application of the natural electric field for detecting karst conduits on Guam: In Beck BF (Ed.) Proceedings of the 5th multidisciplinary conference on sinkholes and the engineering and environmental impacts of karst, Gatlinburg, Tennessee.

Loke, M.H., and Barker, R.D., 1996, Practical techniques for 3D resistivity surveys and data inversion: Geophysical Prospecting, **44**, 499-523.

Loke, M.H., and Lane, J.W., 2002, The use of constraints in 2D and 3D resistivity modelling: Proceedings of the 8th meeting of the EEGS, Aveiro, Portugal.

Maillol, J.M., Seguin, M.K., Gupta, O.P., Akhauri, H.M., and Sen, N., 1999, Electrical resistivity tomography survey for delineating uncharted mine galleries in West Bengal, India: Geophysical Prospecting, **47**, 103-116.

Naudet, V., Revil, A., Bottero, J.Y., and Begassat, P., 2003, Relationship between self-potential (SP) signals and redox conditions in contaminated groundwater: Geophysical Research Letters, **30**, 2091.

Nyquist, J.E., and Corry, C.E., 2002, Self-potential: The ugly duckling of environmental geophysics: The Leading Edge, 446-451.

Ogilvy, R.D., Meldrum, P.I., and Chambers, J.E., 1999, Imaging of industrial waste deposits and buried quarry geometry by 3-D resistivity tomography: European Journal of Environmental and Engineering Geophysics, **3**, 103-113.

Parasnis, D.S., 1997, Principles of applied geophysics 5th Edition: Chapman & Hall, London.

Patella, D., 1997a, Introduction to ground surface self-potential tomography: Geophysical Prospecting, **45**, 653-681.

Patella, D., 1997b, Self-potential global tomography including topographic effects: Geophysical Prospecting, **45**, 843-863.

Patella, D., 1998, Erratum: Geophysical Prospecting, **46**, 103.

Perrone, A., Iannuzzi, A., Lapenna, V., Lorenzo, P., Piscitelli, S., Rizzo, E., and Sdao, F., 2004, High-resolution electrical imaging of the Varco d'Izzo earthflow: Journal of Applied Geophysics, **56**, 17-29.

Quarto, R., and Schiavone, D., 1996, Detection of cavities by the self-potential method: First Break, **14**, 419-431.

Reppert, P.M., and Morgan, F.D., 2003, Temperature-dependent streaming potentials: 1. Theory: Journal of Geophysical Research – Solid Earth, **108**, 2546.

Revil, A., Naudet, V., Nouzaret, J., and Pessel, M., 2003, Principles of electrography applied to self-potential electrokinetic sources and hydrogeological applications: Water Resources Research, **39**, 1114.

Sailhac, P., and Marquis, G., 2001, Analytic potentials for the forward and inverse modeling of SP anomalies caused by subsurface fluid flow: Geophysical Research Letters, **28**, 1851-1854.

Sailhac, P., Marquis, G., Darnet, M. and Szalai, S., 2003, On the characterization of subsurface flow and hydraulic conductivity from surface SP measurements: Correcting for electrical heterogeneities: Geophysical Research Abstracts, **5**, 03429.

Telford, W.M., Geldart, L.P., and Sheriff, R.E., 1990, Applied Geophysics 2nd Edition: Cambridge University Press, Cambridge.

Titov, K., Ilyin, Yu., Konosavski, P., and Levitski, A., 2002, Electrokinetic spontaneous polarization in porous media: petrophysics and numerical modeling: Journal of Hydrology, **267**, 207-216.

van Schoor, M., 2002, Detection of sinkholes using 2D electrical resistivity imaging: Journal of Applied Geophysics, **50**, 393-399.

Vichabian, Y., and Morgan, F.D., 2002, Self potentials in cave detection: The Leading Edge, 866-871.

Wilkinson, P.B., Fromhold, T.M., Tench, C.R., Taylor, R.P. and Micolich, A.P., 2001, Compact fourth-order finite difference method for solving differential equations: Physical Review E, **64**, 047701.

Zhou, W.F., Z., Beck, B.F., and Stephenson, J.B., 1999, Investigation of groundwater flow in karst areas using component separation of natural potential measurements: Environmental Geology, **37**, 19-25.

Zhou, W.F., Beck, B.F., and Adams, A.L., 2002, Effective electrode array in mapping karst hazards in electrical resistivity tomography: Environmental Geology, **42**, 922-928.

Figure 1.   **Plan of sites B and C. The solid geology, the locations of the former colliery buildings and railway, and the boundary of the former spoil heap are highlighted.**

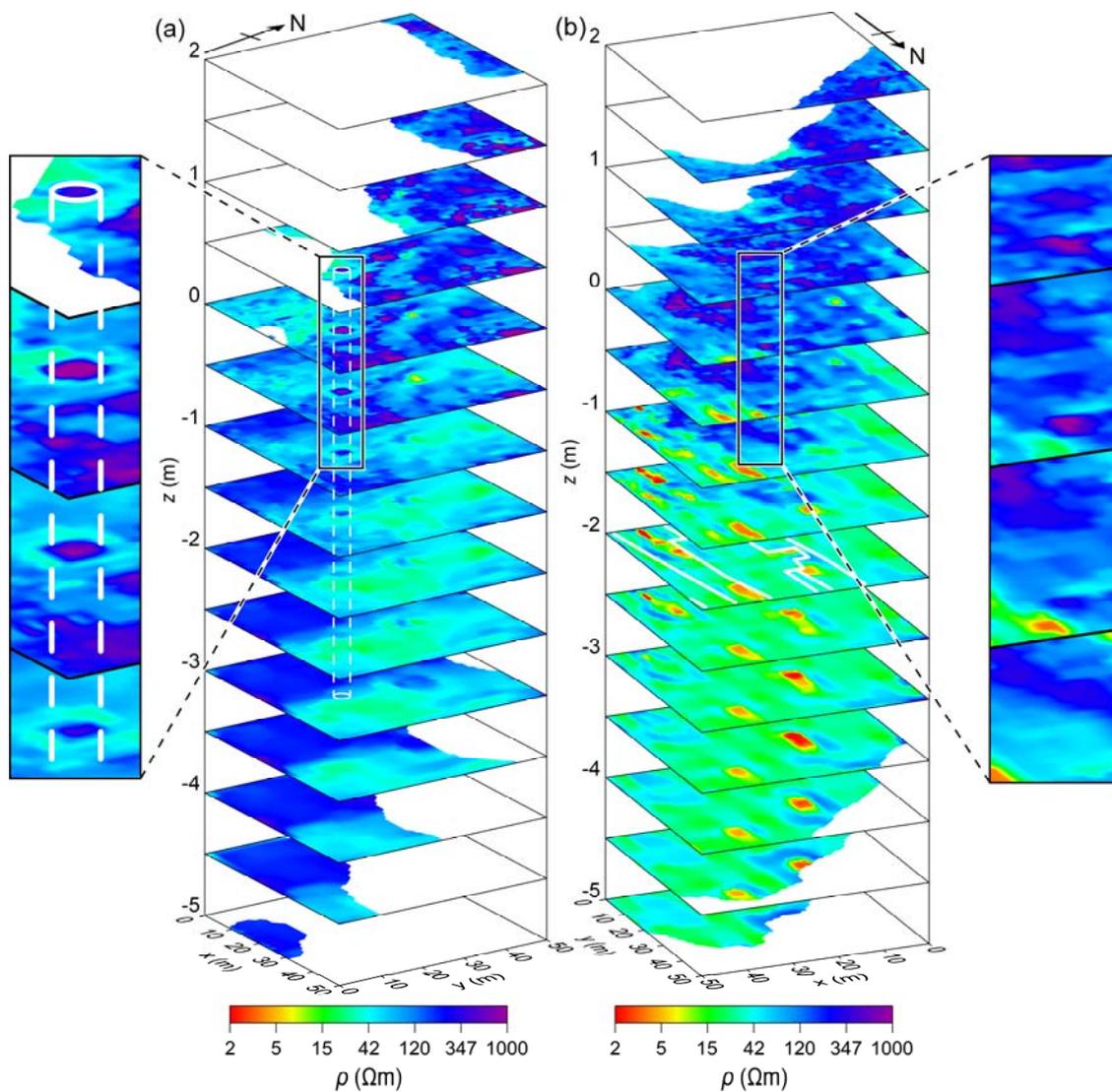**Figure 2.**   **Photographs of (a) Site B and (b) Site C.**

Figure 3. Horizontal slices showing resistivity ρ as a function of (x, y, z) for (a) Site B and (b) Site C. The white regions are either above ground level or below the limits of the model. For Site B, a 3 m diameter cylinder is shown to highlight the mineshaft. For Site C, the former colliery infrastructure is shown by solid white lines. Insets show magnified regions of $\rho(x, y, z)$ in the vicinity of the mineshafts.
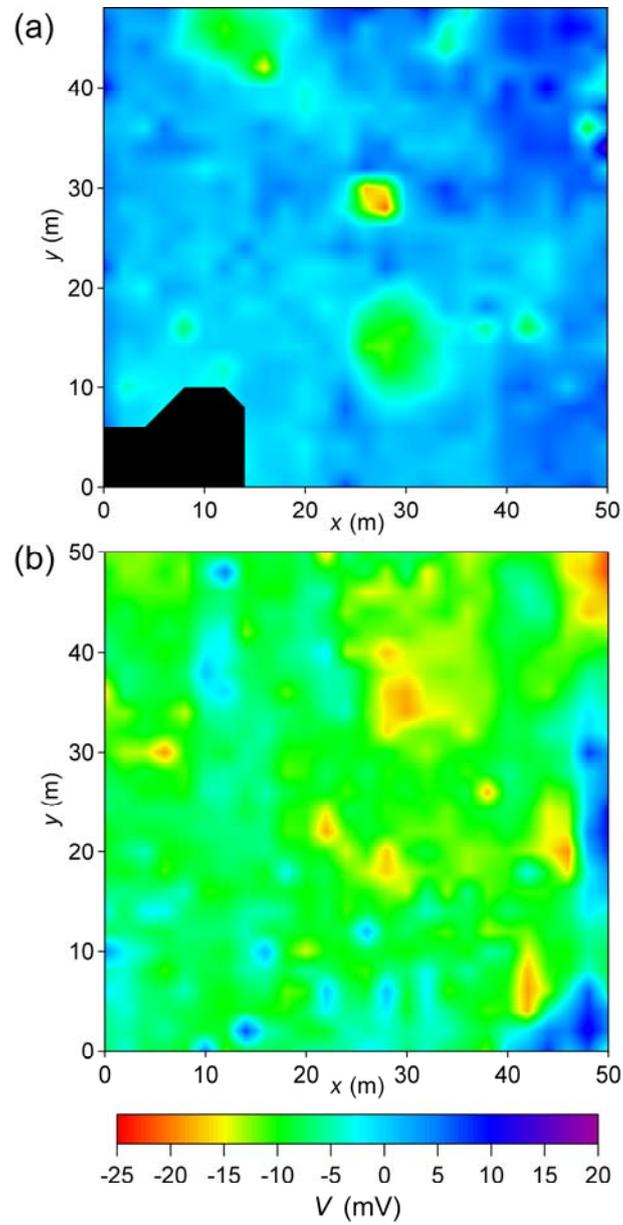
Figure 4. Plots of the self-potential *V* measured at 2 m intervals as a function of (*x, y*) for (a) Site B and (b) Site C. The black region in (a) shows the extent of the gravel road.
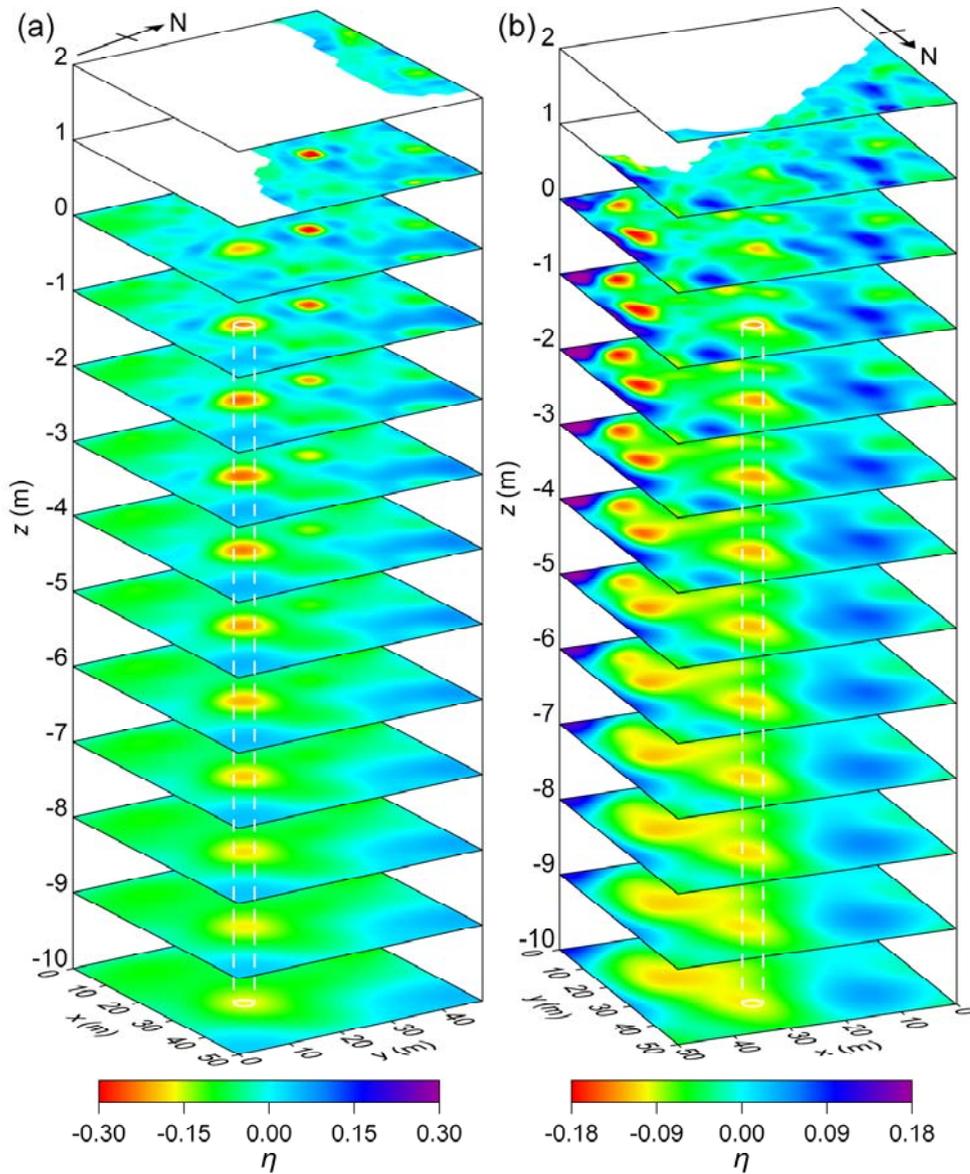
Figure 5. Horizontal slices showing Charge Occurrence Probability η as a function of (*x, y, z*) for (a) Site B and (b) Site C. The white regions indicate points that are above ground level. For each site, a 3 m diameter outline is shown by a dashed white line to highlight the anomalies associated with the mineshafts.
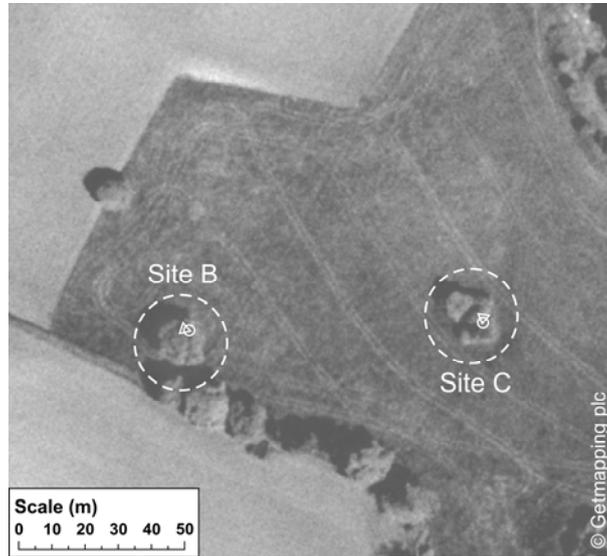
Figure 6. Aerial photograph of both sites before they were prepared for the surveys. Two clumps of trees (circled with white dashed lines) cover the mine entrances. Circles show the locations of the SP shaft anomalies and triangles mark the centers of the shafts on Ordnance Survey maps.